

IMECE2022-94838

ANALYSIS OF SHARK FLUID DYNAMICS TO GUIDE SATELLITE TELEMETRY TAG DEVELOPMENT

Munir Zarea¹, Evan Brown¹, Allen George¹, Joshua Kozsey¹, Tyler Palmgren¹, Meng-Chien Wu¹, Sarah Oman¹, John Parmigiani¹, Joseph Piacenza¹, and Susan Piacenza²

¹School of Mechanical, Industrial, and Manufacturing Engineering, Oregon State University, Corvallis, OR

²Department of Fisheries, Wildlife, and Conservation Sciences, Oregon State University, Corvallis, OR

ABSTRACT

Sharks are powerful predators that make long-range migrations across vast swaths of the ocean. Scientists attach satellite telemetry tracking tags to sharks in order to gather behavior data, and better understand their movement patterns and habitat usage. However, hydrodynamic loading from these tags may unintentionally influence the host shark's behavior, although the extent of the loading is still not well understood. While tag manufacturers have made incremental improvements to make tags lighter and smaller, there is still not a clear understanding between tag design and animal impact. This fundamental knowledge gap makes the design of telemetry tags difficult when aiming to minimize hydrodynamic effects. In this paper, we present an approach intended to help inform tag design. In addition, a case study demonstrates this approach using 3D digital models of four different shark species: the great hammerhead *Sphyrna mokarran*, shortfin mako *Isurus oxyrinchus*, blacktip reef *Carcharhinus limbatus*, and Caribbean reef *Carcharhinus perezii*. Computational fluid dynamics (CFD) methods are used to estimate baseline drag and lift coefficients from a range of angles of attack to simulate the sharks ascending, descending, and swimming horizontally. Lift and drag coefficients are solved through force reports integrated into STAR-CCM+. The simulations were solved with the Menter shear stress transport (SST) $k-\omega$ turbulence model at steady-state. Across the species we examined, the drag and lift coefficients ranged from 0.14 – 0.21 and -0.02 – 0.37, respectively. Plots of pressure distributions and fluid flow associated with each shark's average cruising speeds are presented, providing insight for future researchers investigating optimal tag placement that minimizes the tag's impact. To help validate the computational models, wind tunnel testing was performed by using 3D printed models of each shark, allowing us to empirically

measure lift and drag forces. A three-axis sting-balance style measurement system with strain gauges was used, while considering wind speed, fluid density, and matching Reynolds numbers associated with the CFD models for each species. Finally, a statistical comparison between the computational and wind tunnel measurements was performed. Moving forward, we will explore the changes in drag and lift with different satellite tag models attached to the shark species. Our findings will create a method to help quantify the hydrodynamic impact of different tag designs on sharks. This can be used by future researchers to determine the lift and drag forces a shark experiences with a satellite telemetry tag attached. Ultimately, this information will help to better monitor sharks in their natural environment and provide information that can be useful to the conservation of the species.

NOMENCLATURE

CFD	Computational Fluid Dynamics
SST	Shear Stress Transport
CAD	Computer Assisted Design
3D	Three Dimensional
TL	Total Length
ABS	Acrylonitrile Butadiene Styrene
PA12	Polymide 12 (Nylon)

1 INTRODUCTION

Many species of sharks make oceanic basin-wide migrations, and, as apex predators, control food webs across a range of ecosystems. Most of our knowledge of shark spatial movements is derived from satellite telemetry tags, which are especially

helpful for studying movement patterns of highly migratory marine fauna [1] [2]. While satellite telemetry has revealed exciting insights into marine spatial ecology, logistical problems can limit their overall utility [3–5]. For example, tag transmission duration is limited by battery power, antenna robustness, biofouling, and limited attachment duration [6–8]. In addition, satellite tags induce drag, which can cause behavioral shifts that may not represent natural movements in untagged individuals [9] [10]. The extent of hydrodynamic loading across marine taxa is still not well understood. While tag manufacturers have made incremental improvements to make tags lighter and smaller, there is still not a clear understanding between tag design and animal impact. This fundamental knowledge gap makes the design of telemetry tags difficult when aiming to minimize hydrodynamic effects.

The aim of this research is to create a repeatable approach toward measuring the hydrodynamic impact of satellite tags on marine animals. Our case study uses computational fluid dynamics (CFD) models of the four different shark species, followed by wind tunnel testing to estimate coefficients of drag and lift, intended to validate and tune the CFD models. Our work is intended to contribute to the understanding of shark hydrodynamics, and will create a methodology that can be used by future researcher's to expand the existing knowledge base. In the future, our validated CFD modeling method can be used to test novel satellite telemetry tag designs that are more hydrodynamically efficient and produce less of an impact on the animal. In turn, these improved tags can provide more representative data on shark migration patterns, habitats, and energetics.

2 BACKGROUND

In research and conservation, telemetry tags are frequently used to track shark movements and habitat locations. However, the effect of these tags on the host shark's energy expenditure and behavior is not well understood and requires further research. Telemetry tags range in size from small solar-powered satellite tags to large animal-borne camera tags, relative to the shark, and may induce significant amounts of drag (Fig. 1). If excessive, this extra loading on the shark could affect its behavior and bring the validity of the data into question.

The use of CFD models in the biological sciences is generally underutilized, and specifically even more so for sharks. However, some CFD research has involved shark species. For example, CFD modelling has been used to model specific anatomical features, such as the a hammerhead cephalofoil (Gaylord [12], shortfin mako skin in Diez [13], a Toste shark hydrofoil in Muratoglu [14] and 3D printing and testing panels of scaled up shark skin to observe their unique hydrodynamic properties such as in Bechert [15]. As such, full body CFD models of sharks are quite limited; although, this has been explored with other animals, such as seals and sea turtles [16–18]. In Kelly et al. [16], green sea turtles were modeled with and without tags, using a



FIGURE 1. CATCAM ANIMAL BORNE CAMERA ATTACHED TO A GREY REEF SHARK DORSAL FIN. PHOTO REPRODUCED FROM J. MOURIER [11].

3D scan of a stranded juvenile green sea turtle and CAD models of existing satellite tags. However, full-body 3D models of live sharks have been difficult to obtain, since obtaining photos or video to run photogrammetry software could pose dangerous and potentially deadly risks to the animals and humans involved. Until recently, 3D models of sharks that do exist are not a high enough quality to run accurate simulations with, and as a result do not yield meaningful CFD data [19]. However, recent advancements in underwater photogrammetry now permit full body 3D scans of living organisms [20].

3 GENERAL METHOD

A high-level overview of our approach is shown in Fig. 2, further detailed in the subsections below.

3.1 CFD Modeling

Photogrammetry models of the four species provided by DigitalLife3D [21] were imported into STAR-CCM+ for creation of the fluid domain boundaries. To minimize any influence of the wall boundaries on the flow near the shark, the surrounding walls were placed approximately 3 m away from the shark. The inlet and outlet boundaries were placed approximately 5.25 m away from the head and tail, respectively. The velocity of the inlet boundary was set to the corresponding shark's average swimming speed [5, 22, 23].

An initial polyhedral mesh with a base size of 0.05 m was generated with the STAR-CCM+ automated mesher, with a mesh refinement zone set around the shark's immediate vicinity. To validate this base size as a suitable starting point for the models, a mesh refinement process was followed building on work by Rygg et al. [23]. The mesh base size for the Blacktip CFD model was reduced by 0.02 m to approximately double the mesh cell count from 1 to 2 million cells, and the reported lift and drag forces were seen to have less than 3% difference from the 1 million cell results, reflecting mesh-independent results (Fig. 3). To accurately resolve the pressure and shear forces on the shark, at least 10 prism layers were created at 33% of the mesh base

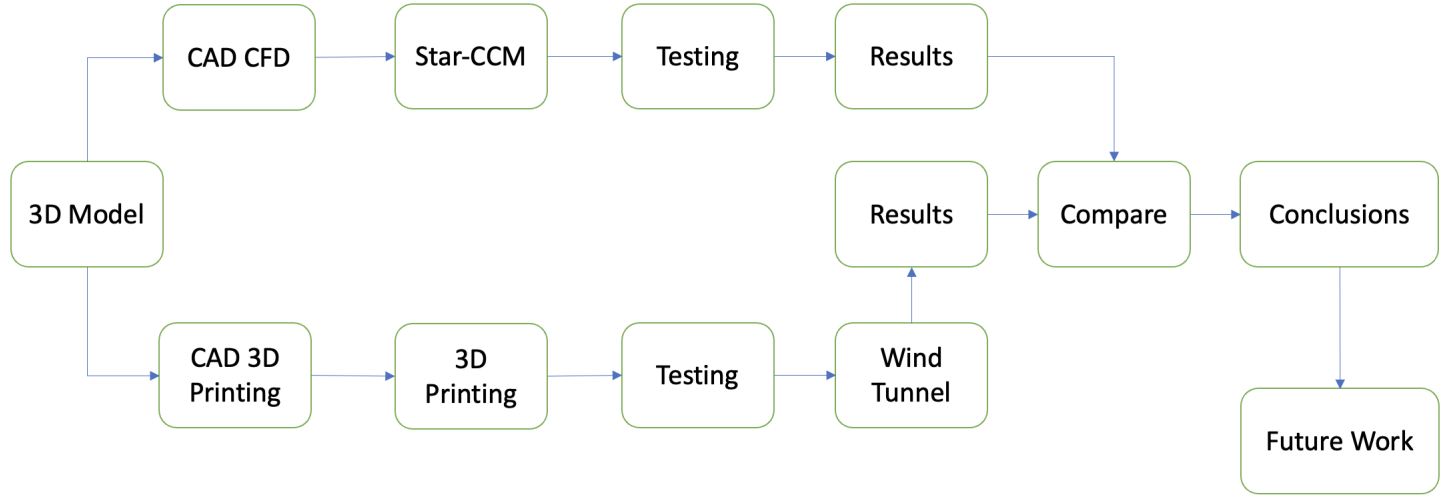


FIGURE 2. GENERAL METHODOLOGY FLOW CHART.

size. The number of prism cells was increased and/or the base size was decreased until most cells on the model's boundary had $y^+ < 1$. [24]. The mesh cell count for each CFD model varied from approximately 1 to 3 million cells.

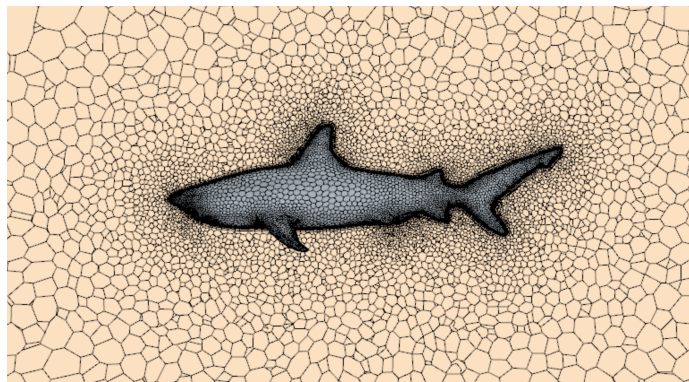


FIGURE 3. MESH OF BLACKTIP 0° CFD MODEL GENERATED IN STAR-CCM+. DEFAULT POLYGONAL MESHER WAS USED WITH BASE SIZE OF 0.05 METERS.

All CFD models were solved with a Menter Shear Stress Transport (SST) $k-\omega$ model with a segregated flow solver. The solution was evaluated at steady state with incompressible seawater ($\mu = 1.027 * 10^{-3}$ $\text{Pa} \cdot \text{s}$, $\rho = 1023 \text{ kg} \cdot \text{m}^{-3}$), and was iterated until normalized residuals for all fields (x-momentum, turbulent kinetic energy, etc.) were below $2 * 10^{-3}$, typically

achieved by 1250 iterations. To confirm force convergence, lift and drag forces on the shark were recorded for an additional 75 iterations and confirmed to not vary by more than 5% of the mean force [24].

3.2 Wind Tunnel Experimental Design

Wind tunnel testing for lift and drag force measurement was conducted in an AEROLAB Educational Wind Tunnel at Oregon State University, with a provided sting force balance. The force balance outputted to 3 load cell amplifiers, each of which measured axial force, vertical force, and pitching moment, respectively. The amplifiers were connected to an Arduino Nano, which outputted the readings over USB for data collection and analysis.

In order to utilize the supplied CAD models for 3D printing, we made minor adjustments to the files, such as completing surfaces to allow for a smoother boundary and thus, less complex fluid flow conditions. From here, the models were 3D printed with ABS in an Ultimaker S5, as well as Nylon PA12 courtesy of HP. After initial testing, additional no-tail models were printed in ABS that lacked the tail geometry of the shark. In order to accommodate the size of the sharks needed for the wind tunnel, the prints for the full ABS versions were separated into three sections: the head, the body, and the tail. Each piece was adhered together with JB Weld and applied with Bondo putty to attempt to achieve a smooth finish, shown in (Fig. 7).

Before testing the 3D-printed shark models, the force balance output was calibrated. To calibrate the normal force and pitching moment output, the force balance was outfitted with

a 3D-printed sleeve with 8 regularly spaced slots for hanging masses, shown in Fig. 4. The force balance was then mounted horizontally on a vise and various known masses were hung from the sleeve. The force balance output was recorded for each trial, and yielded a constant factor to convert the output to the known forces and moments. For calibrating the axial force output, the force balance was mounted vertically and outfitted with another sleeve that provided a flat platform to place objects on. Various known masses were then placed on the sleeve's platform, and the same procedure was followed to yield a constant factor that converts to axial force.



FIGURE 4. CALIBRATION METHOD FOR NORMAL FORCE AND PITCHING MOMENT.

After calibration, each shark's 3D-printed model was mounted on the force balance using a machined aluminum sleeve with a set screw (Fig. 5) and placed into the wind tunnel. The force balance was tared prior to turning the wind tunnel on such that the model's weight was not included in the axial and normal force outputs. The wind tunnel was then set to a speed for the Reynolds number to match the Reynolds number used in the CFD models,

$$Re = \frac{\rho VL}{\mu} \quad (1)$$

Where L is the head-to-tail length of the shark model, V is the fluid velocity, ρ is the fluid density, and μ is the fluid dynamic viscosity.

Trials were run for 2 minutes, and the average readings were then converted to forces with the force balance calibration data. This process was performed for all 3 orientations of each species,



FIGURE 5. MACHINED ALUMINUM SLEEVE WITH SET SCREWS.

using the force balance's controls to manipulate the angle of attack.

As the force balance was inserted into the models at an angle, the recorded normal and axial forces (F_N and F_A) were transformed to drag and lift forces (F_D and F_L) by coordinate rotation. The offset angle θ was measured with a digital protractor.

$$F_D = F_A \cos(\theta) + F_N \sin(\theta) \quad (2)$$

$$F_L = F_N \cos(\theta) - F_A \sin(\theta) \quad (3)$$

3.3 Compare CFD to Wind Tunnel Data

With flow conditions between the CFD models and wind tunnel tests normalized through Reynolds numbers, results were compared through drag and lift coefficients, C_D and C_L .

$$C_D = \frac{2F_D}{\rho V^2 A} \quad (4)$$

$$C_L = \frac{2F_L}{\rho V^2 A} \quad (5)$$

Where ρ is the fluid density, V is the fluid velocity, and A is the frontal area projected in the flow's direction. Accuracy of the CFD model was evaluated by percent error from the wind tunnel

results:

$$\text{Percent Error} = \frac{C_{\text{tunnel}} - C_{\text{CFD}}}{C_{\text{tunnel}}} \cdot 100 \quad (6)$$

Where C is the lift or drag coefficient for a given species.

The results of the wind tunnel testing will then be compared to the results of the CFD simulations. To demonstrate the effectiveness of this method, a sphere was subjected to wind tunnel testing and CFD, as the geometry of a sphere has very predictable flow effects.

3.4 CFD Model Tuning

If any CFD models have a high percent error (i.e. $\geq 10\%$) to the observed lift and drag coefficients in the wind tunnel, several parameters can be adjusted to increase the CFD model accuracy [25] [26]. A Gamma-Re Theta transition model can be applied, such that solver does not model the flow as fully turbulent everywhere. The mesh size can be refined to a smaller base size, or the mesh's boundary prism layer around the shark can be altered to a thinner or thicker height. Since these parameter adjustments can increase computational demand, we performed this process iteratively until a converged, accurate, and computationally feasible CFD solution was found.

4 CASE STUDY AND PRELIMINARY RESULTS

We conducted the wind tunnel and CFD modelling for 4 species of shark: the shortfin mako *Isurus oxyrinchus*, the blacktip reef *Carcharhinus limbatus*, the Caribbean reef *Carcharhinus perezii*, and the great hammerhead *Sphyrna mokarran*. These species each had 3D photogrammetric models freely available at DigitalLife 3D repository [21]. While all sharks are top-level predators, each of these species has distinct ecological roles. Shortfin makos are fast swimming open sea species, while blacktip reef and Caribbean reefs sharks inhabit complex benthic reef communities, and are agile swimmers through reef troughs or crests. Great hammerhead sharks are cosmopolitan and occur in variety of nearshore and offshore habitats, including reefs, lagoons, and deep water, while powerful swimmers, the unusual cephalofoil (hammer) head can induce increased drag, but is suspected to aid in prey detection.

4.1 Shark Specific Model

In order to closely mimic a shark moving through water in the wind tunnel and CFD models, we considered nominal swim cruising speed. The cruising speed was chosen to represent the speed at which the individual species of shark spends most of its time (Tab. 1). As this study was focused on the shape of the shark, rather than the size and age, we used the total body

lengths and cruising speeds of adult sharks gathered from peer reviewed articles [27–30]. This allowed us to more accurately model average cruising speed and average length in consideration of hydrodynamic forces (Fig. 6). For this study, we ignored maximum swim speed, commonly referred to as attack speed, as this speed is only attained for a short duration, while the shark is actively attacking its prey.

TABLE 1. SHARK CHARACTERISTICS USED IN WIND TUNNEL AND CFD MODELS. TOTAL LENGTHS FROM [27–30], CRUISING SPEEDS FROM [12, 22, 23]

Shark	Frontal Area (m^2)	Average Cruising Speed (m/s)	Average Total Length (TL) (m)	Re. No.
Blacktip Reef	4.87E-02	0.520	1.50	7.42E+05
Shortfin Mako	0.524	0.540	2.20	1.13E+06
Caribbean Reef	0.136	0.610	2.50	1.45E+06
Great Hammerhead	0.335	0.900	4.00	3.43E+06

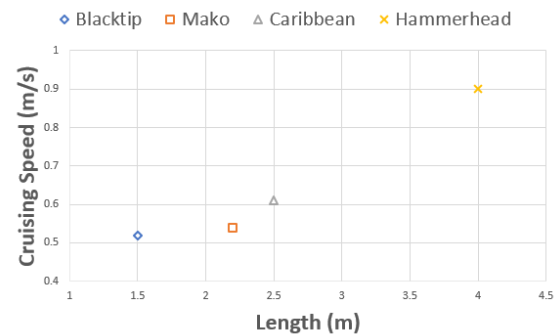


FIGURE 6. THE RELATIONSHIP OF SHARK LENGTH AND CRUISING SPEED.

We conducted both the wind tunnel and CFD modelling using three angles of attack for each shark: -12° , 0° , and 12° from horizontal. These angles best represent the shark descending, swimming horizontally, and ascending, respectively [12]. While

there are dynamic aspects to a shark's motion, such as body flexion while swimming, we ultimately chose to ignore this to focus this current research on developing a baseline understanding on hydrodynamic forces on the shark species-specific morphology, however, it will be considered in future work. Thus we treat the sharks as static objects, similar to airplanes, which can still yield data that can still be useful in finding the drag and lift present as sharks travel through the water.



FIGURE 7. BLACKTIP SHARK IN WIND TUNNEL AT 0 DEGREES (HORIZONTAL SWIMMING ANGLE).

4.2 Wind Tunnel

The 3D printed models of each shark species all have mounting holes measured at 15° relative to horizontal (Fig. 7). This means that in order for the shark to be at a horizontal swimming angle, the sting angle must be equal to the mounting hole. For instance, adjusting for the desired 12° angle of the shark, the sting must be angled at 27° . The specificity of these angles were chosen such that the sting will not obstruct other features of the body morphology. For the no-tail models, the sting hole was placed in line with the sharks, to determine if the angle had significant effects on the error between the wind tunnel results and CFD models.

The sting mechanism in the AEROLAB wind tunnel can be adjusted to accommodate the three prescribed angles of attack. There is a potentiometer that measures the angle of the sting-mount mechanism, but with the Arduino data acquisition system, there is no connection for this measurement tool. Instead, the use of a digital protractor provided accurate angles for testing. The location of the sting hole in the shark body is dependant on the shark placement in the test section of the wind tunnel. In order

for the body of the shark to have clearance to adjust the angles of attack accordingly, the sting hole is placed on the underside of the shark body. This allowed the full body of the specimen to be within the boundaries of the test section. Additionally, we chose this position to prevent obstructions when adjusting the angles.

Force coefficients from the wind tunnel tests were compared to the CFD models by percent error and are summarized in Table 3. Results from both the Nylon PA12 and ABS models were recorded to ensure surface finish was not a significant factor in the error of the CFD results.

4.3 CFD Model

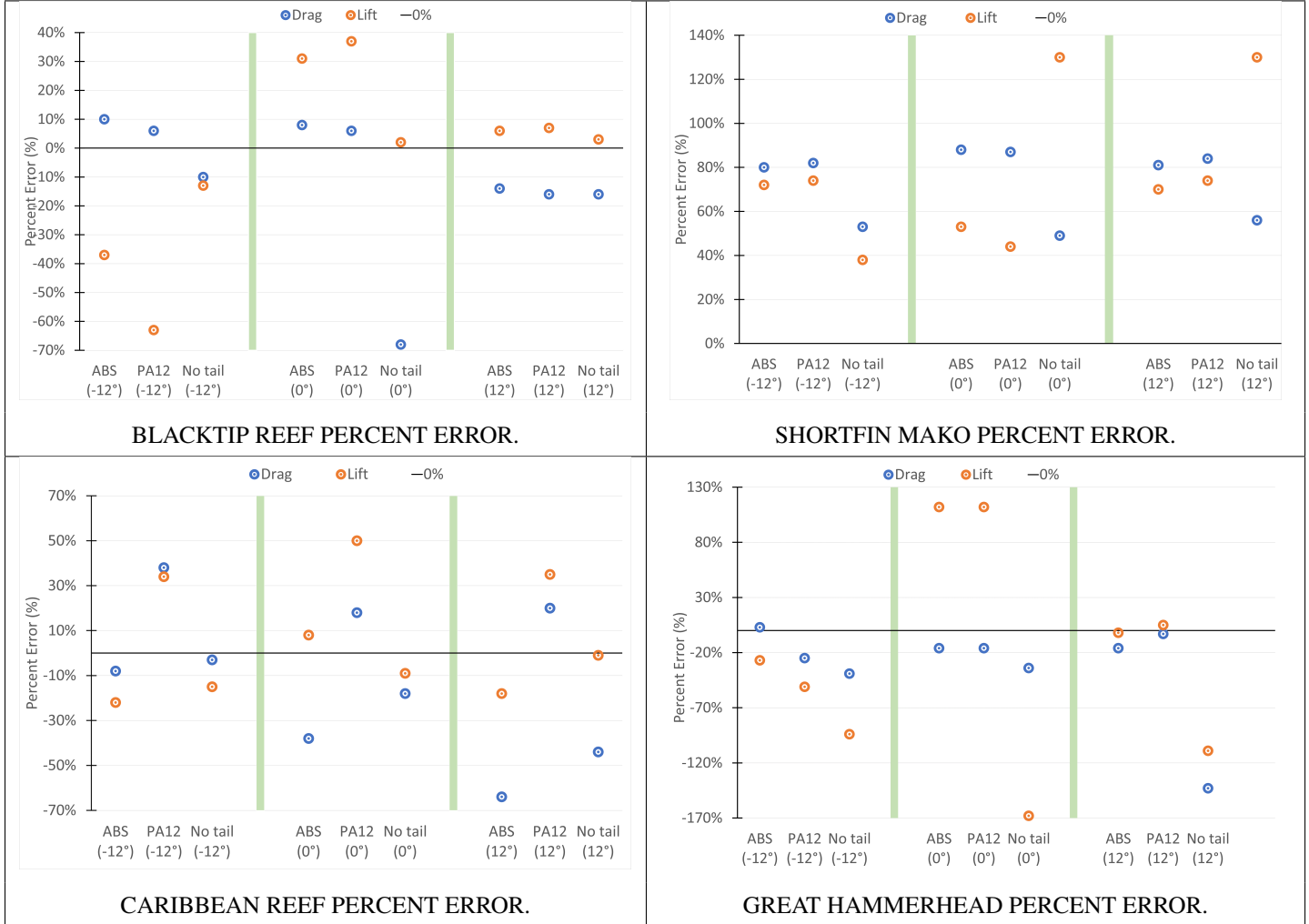
The lift and drag coefficients for each shark were derived in STAR-CCM+ software (version 2021.3) [24], using characteristics from Table 1. We visualized the pressure distributions and streamlines as modelled in STAR-CCM+ for the shark species (Fig. 4). The sharks experienced the highest pressure at their noses and fin edges and the lowest pressures after the fin edges.

Across the species, the coefficient of drag ranged from 5.07×10^{-3} - 0.396, for shortfin mako and Caribbean reef shark, respectively (Tab.2). The coefficient of lift ranged from 2.20×10^{-2} - 0.210, for shortfin mako and great hammerhead, respectively (Tab. 2). The drag coefficients ranged over the angles of attack for the four species. Across all the species, drag was lowest for 0° angle of attack, α , but varied by species whether -12° or 12° had the highest value (Fig. 8). The coefficient of drag varied with frontal area and angle of attack, where the shortfin mako had the largest frontal area, but lowest drag coefficient, relative to angle of attack (Fig. 9).

TABLE 2. DRAG COEFFICIENTS FOR ANGLES OF ATTACK FOR EACH SHARK SPECIES.

Shark	Drag Coefficient at $\alpha = -12^\circ$	Drag Coefficient at $\alpha = 0^\circ$	Drag Coefficient at $\alpha = 12^\circ$
Blacktip	0.222	0.168	0.330
Shortfin Mako	0.151	2.20E-02	5.07E-03
Caribbean	0.221	0.183	0.396
Great Hammerhead	0.406	0.210	0.338

TABLE 3. PERCENT ERROR OF DRAG & LIFT COEFFICIENTS BETWEEN WIND TUNNEL RESULTS AND CFD SIMULATIONS.



4.4 Comparing Wind Tunnel and CFD Results

After calibrating the wind tunnel using the sphere model, all four shark species were tested within the wind tunnel and CFD in three categories: ABS, Nylon PA12, and no-tail. In general, there is correspondence in estimates of drag coefficient from wind tunnel testing and CFD models (Fig. 10). The percent errors shown in Table 3 are separated by shark and subdivided into their respective production methods. The black lines show a 0% error baseline. These results show a semi-clear correlation between the drag coefficients when comparing the ABS and the PA12 models.

The results don't have general trends, so different sources of error need to be discussed. The largest source of error is assumed to be equipment error, due to the neglected condition of the wind tunnel and sting balance, which gave sporadic and potentially faulty data acquisition. This project is based on the idea of similitude, in which real world seawater swimming conditions were simulated with high speed air flows. Surface finish was found

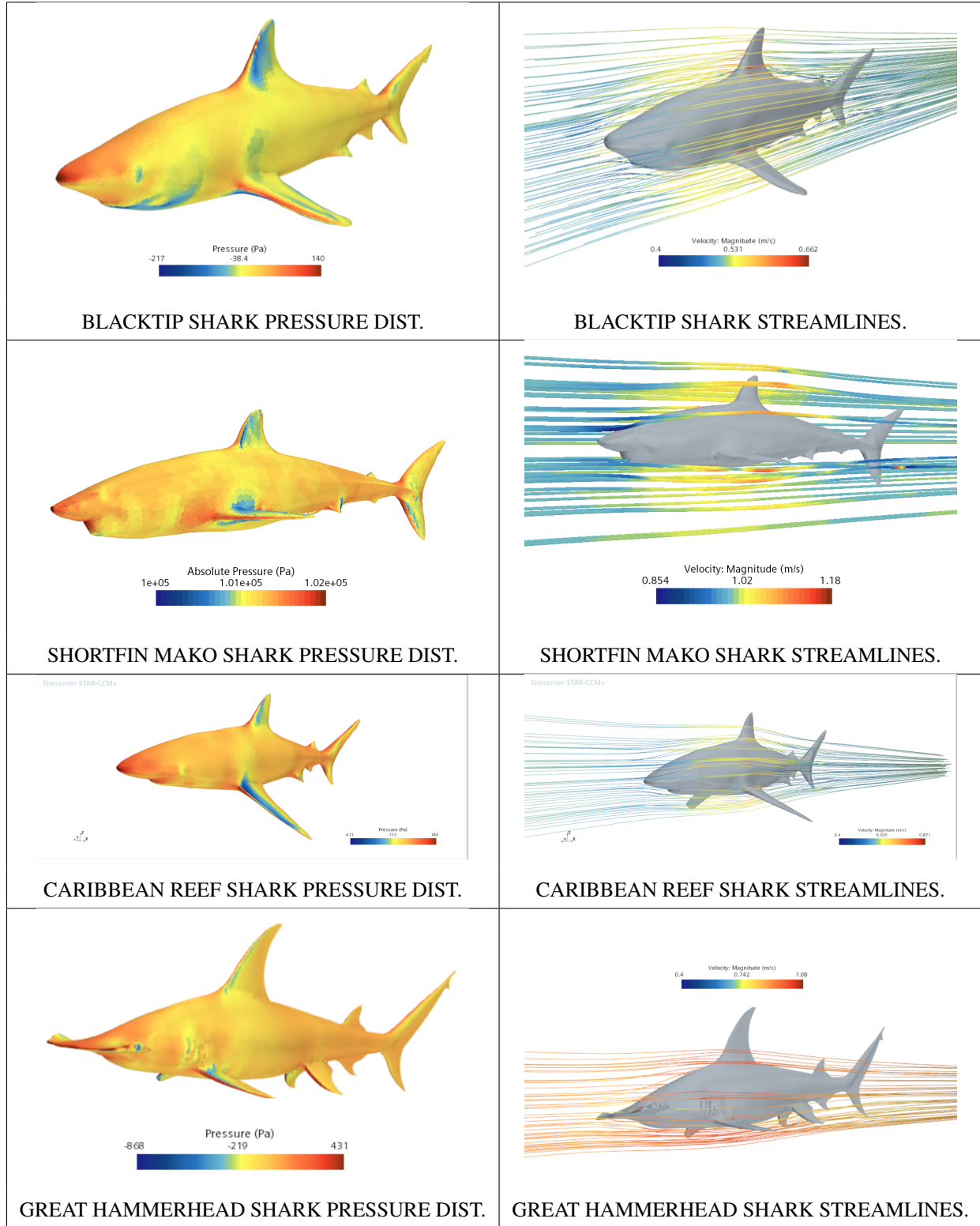
to be generally negligible, since all but the Caribbean reef shark the ABS and PA12 models had similar results, despite the PA12 models being significantly smoother. On top of this the CFD models are unable to simulate the surface finish of the sharks.

In the CFD models, the mesh size could have possibly not been small enough to accurately capture the forces on the shark. The turbulence model used, $k - \omega$ SST, could have also been unsuitable for the application. Not modeling turbulence transition and unsteady flow effects could have additionally led to some error.

5 CONCLUSION

Here, we present a method to evaluate the hydrodynamic forces on sharks using experimental wind tunnel tests to validate and tune CFD models of biological organisms. This approach can be used to compare hydrodynamic forces across species. Im-

TABLE 4. PRESSURE DISTRIBUTIONS AND STREAMLINES FOR EACH SHARK SPECIES.



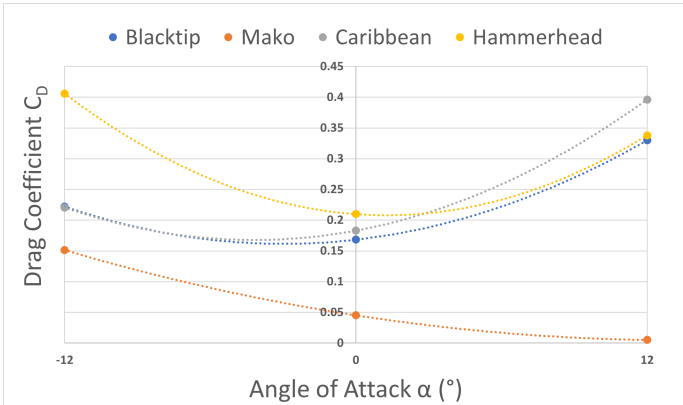


FIGURE 8. RELATIONSHIP BETWEEN DRAG COEFFICIENT AND ANGLE OF ATTACK OF EACH SHARK (CFD RESULTS ONLY).

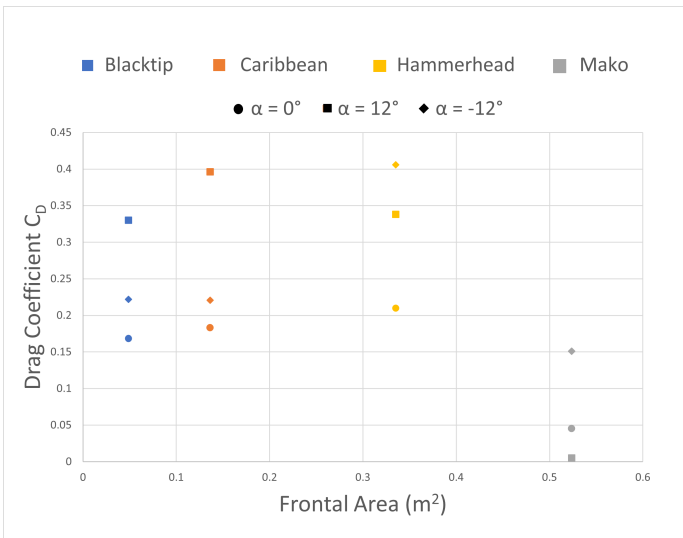


FIGURE 9. RELATIONSHIP BETWEEN DRAG COEFFICIENT AND FRONTAL AREA (m^2) OF EACH SHARK SPECIES.

pacts of bio-logging tags on sharks is not well understood [31], but this approach can be used to evaluate how satellite tags could influence hydrodynamics, and consequently behavior [10]. The CAD model, computational models, and wind tunnel data in this research can aid the exploration of satellite tag designs for sharks. Drag and lift coefficients in CFD modeling and wind tunnel testing will provide insight into shark hydrodynamics and we can use this information to compare the results and further guide tag design.

From the sphere results, outside of the lowest Reynolds number, the results between CFD and wind tunnel testing vary slightly. Changes in temperature can create error in the calculation of drag coefficient for wind tunnel results. Higher temperatures and humidity will lead to changes in air density and

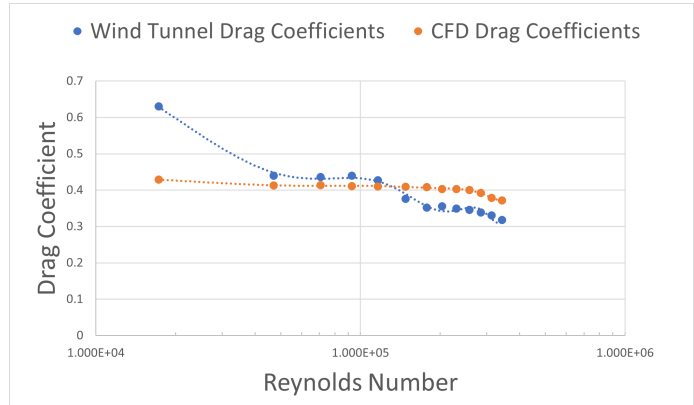


FIGURE 10. COEFFICIENTS OF DRAG FOR SPHERE AT DIFFERENT REYNOLDS NUMBERS FROM WIND TUNNEL TESTING AND CFD SIMULATIONS.

viscosity, which may explain the variation between the CFD and wind tunnel results. Another trend in error was during exceptionally high wind speed tests. This caused the tunnel system to vibrate during operation, which could have affected data collection. In addition, for wind tunnel testing, the 3D printed shark models have a slight surface texture that may induce microturbulence that could influence the hydrodynamic forcing as measured. Lastly, with the age and uncertainty of the wind tunnel components, the wind speed may have been inaccurate. Speed was calculated by translating from Hertz, given by the display on the wind tunnel, to a velocity that was useful to us. Alternate methods could have been implemented such as a pressure transducer to convert the change in pressure through the test section to meters per second.

The ultimate goal of this research is to design low-impact satellite tags. The next steps include comparing the hydrodynamic results of tagged sharks and tagged individuals to optimize the tag design. Using CAD software to model the newly designed tag, we will also meet the basic functionality of the satellite tag at the same time. Designing satellite tags that minimize hydrodynamic impacts should result in higher fidelity tracking data that can advance shark research and conservation.

REFERENCES

- [1] Hart, K., and Hyrenbach, K., 2009. "Satellite telemetry of marine megavertebrates: the coming of age of an experimental science". *Endangered Species Research*, **10**, Dec., pp. 9–20.
- [2] Shillinger, G., Bailey, H., Bograd, S., Hazen, E., Hamann, M., Gaspar, P., Godley, B., Wilson, R., and Spotila, J., 2012. "Tagging through the stages: technical and ecological challenges in observing life histories through biologging". *Marine Ecology Progress Series*, **457**, June,

- pp. 165–170.
- [3] Block, B. A., Jonsen, I. D., Jorgensen, S. J., Winship, A. J., Shaffer, S. A., Bograd, S. J., Hazen, E. L., Foley, D. G., Breed, G. A., Harrison, A.-L., Ganong, J. E., Swithenbank, A., Castleton, M., Dewar, H., Mate, B. R., Shillinger, G. L., Schaefer, K. M., Benson, S. R., Weise, M. J., Henry, R. W., and Costa, D. P., 2011. “Tracking apex marine predator movements in a dynamic ocean”. *Nature*, **475**(7354), July, pp. 86–90.
 - [4] Costa, D. P., Breed, G. A., and Robinson, P. W., 2012. “New Insights into Pelagic Migrations: Implications for Ecology and Conservation”. *Annual Review of Ecology, Evolution, and Systematics*, **43**(1), Dec., pp. 73–96.
 - [5] Godley, B., Blumenthal, J., Broderick, A., Coyne, M., Godfrey, M., Hawkes, L., and Witt, M., 2008. “Satellite tracking of sea turtles: Where have we been and where do we go next?”. *Endangered Species Research*, **4**, Jan., pp. 3–22.
 - [6] Mansfield, K. L., Wyneken, J., Rittschof, D., Walsh, M., Lim, C. W., and Richards, P. M., 2012. “Satellite tag attachment methods for tracking neonate sea turtles”. *Marine Ecology Progress Series*, **457**, June, pp. 181–192.
 - [7] Piacenza, J., Piacenza, S., Mayoral, S., Kenney, A., and Shields, N., 2018. “Design Opportunities for Sea Turtle Satellite Tracking Devices”. In Volume 4: 23rd Design for Manufacturing and the Life Cycle Conference; 12th International Conference on Micro- and Nanosystems, American Society of Mechanical Engineers, p. V004T05A024.
 - [8] Hart, K. M., Guzy, J. C., and Smith, B. J., 2021. “Drivers of realized satellite tracking duration in marine turtles”. *Movement Ecology*, **9**(1), Dec., p. 1.
 - [9] Todd Jones, T., Van Houtan, K. S., Bostrom, B. L., Ostafichuk, P., Mikkelsen, J., Tezcan, E., Carey, M., Immlach, B., and Seminoff, J. A., 2013. “Calculating the ecological impacts of animal-borne instruments on aquatic organisms”. *Methods in Ecology and Evolution*, **4**(12), Dec., pp. 1178–1186.
 - [10] O’Connell, D., Kehl, C. E., Taylor, B. K., Piacenza, J., Piacenza, S., and Faller II, K. J., 2021. “A computational framework for studying energetics and resource management in sea turtle migration and autonomous systems”. *Journal of Theoretical Biology*, **527**, Oct., p. 110815.
 - [11] johannmourier, 2017. GOMBESSA IV Expedition – Revealing reef shark behaviour as never seen before!, Aug.
 - [12] Gaylord, M. K., Blades, E. L., and Parsons, G. R., 2020. “A hydrodynamics assessment of the hammerhead shark cephalofoil”. *Scientific Reports*, **10**(1), Sept., p. 14495.
 - [13] Díez, G., Soto, M., and Blanco, J. M., 2015. “Biological characterization of the skin of shortfin mako shark *Isurus oxyrinchus* and preliminary study of the hydrodynamic behaviour through computational fluid dynamics: hydrodynamics of *isurus oxyrinchus* skin”. *Journal of Fish Biology*, **87**(1), July, pp. 123–137.
 - [14] Muratoğlu, A., 2019. “Hydrodynamic Analysis of Shark Body Hydrofoil Using CFD Methods”. *International Journal of Engineering Research and Development*, **11**(1), Jan., pp. 226–238.
 - [15] Bechert, D. W., Bruse, M., and Hage, W., 2000. “Experiments with three-dimensional riblets as an idealized model of shark skin”. *Experiments in Fluids*, **28**(5), May, pp. 403–412.
 - [16] Kelly, B., Nguyen, K., Miles, Z., Mayoral, S., Piacenza, S., Zhang, C., and Piacenza, J., 2019. “Exploring Design Trades to Extend Useful Life of Platform Terminal Transmitters on Sea Turtles”. In IDETC-CIE2019.
 - [17] Kay, W. P., Naumann, D. S., Bowen, H. J., Withers, S. J., Evans, B. J., Wilson, R. P., Stringell, T. B., Bull, J. C., Hopkins, P. W., and Börger, L., 2019. “Minimizing the impact of biologging devices: Using computational fluid dynamics for optimizing tag design and positioning”. *Methods in Ecology and Evolution*, **10**(8), Aug., pp. 1222–1233.
 - [18] Kyte, A., Pass, C., Pemberton, R., Sharman, M., and McKnight, J. C., 2019. “A computational fluid dynamics (CFD) based method for assessing the hydrodynamic impact of animal borne data loggers on host marine mammals”. *Marine Mammal Science*, **35**(2), Apr., pp. 364–394.
 - [19] Chapple, T., 2022. Interview with Dr. Chapple, of the OSU College of Agricultural Sciences regarding existing shark telemetry tags, Feb.
 - [20] Irschick, D. J., Martin, J., Siebert, U., Kristensen, J. H., Madsen, P. T., and Christiansen, F., 2021. “Creation of accurate 3D models of harbor porpoises (*Phocoena phocoena*) using 3D photogrammetry”. *Marine Mammal Science*, **37**(2), Apr., pp. 482–491.
 - [21] Digital Life 3D. Digital Life.
 - [22] Jacoby, D. M. P., Siriwat, P., Freeman, R., and Carbone, C., 2015. “Is the scaling of swim speed in sharks driven by metabolism?”. *Biology Letters*, **11**(12), Dec., p. 20150781.
 - [23] Rygg, A. D., Cox, J. P. L., Abel, R., Webb, A. G., Smith, N. B., and Craven, B. A., 2013. “A Computational Study of the Hydrodynamics in the Nasal Region of a Hammerhead Shark (*Sphyrna tudes*): Implications for Olfaction”. *PLoS ONE*, **8**(3), Mar., p. e59783.
 - [24] Siemens Digital Industries Software, 2021. Simcenter \uppercaseSTAR-CCM+, version 2021.1.
 - [25] Tian, R., Li, L., Wang, W., Chang, X., Ravi, S., and Xie, G., 2020. “CFD based parameter tuning for motion control of robotic fish”. *Bioinspiration & Biomimetics*, **15**(2), Feb., p. 026008.
 - [26] Martins, N. R., and da Graça, G. C., 2016. “Validation of numerical simulation tools for wind-driven natural ventilation design”. *Building Simulation*, **9**(1), Feb., pp. 75–87.
 - [27] Chin, A., Tobin, A. J., Heupel, M. R., and Simpfendorfer, C. A., 2013. “Population structure and residency patterns of the blacktip reef shark *Carcharhinus melanopterus*

- in turbid coastal environments: *carcharhinus melanopterus* populations in coastal habitats". *Journal of Fish Biology*, **82**(4), Apr., pp. 1192–1210.
- [28] Tavares, R., 2009. "Fishery biology of the Caribbean reef sharks, *Carcharhinus perezi* (Poey, 1876), in a Caribbean insular platform: Los Roques Archipelago national park, Venezuela". *Pan-American Journal of Aquatic Sciences*, **4**, Jan., pp. 500–512.
- [29] Piercy, A. N., Carlson, J. K., and Passerotti, M. S., 2010. "Age and growth of the great hammerhead shark, *Sphyrna mokarran*, in the north-western Atlantic Ocean and Gulf of Mexico". *Marine and Freshwater Research*, **61**(9), Sept., pp. 992–998.
- [30] Bishop, S. D. H., Francis, M. P., Duffy, C., and Montgomery, J. C., 2006. "Age, growth, maturity, longevity and natural mortality of the shortfin mako shark (*Isurus oxyrinchus*) in New Zealand waters". *Marine and Freshwater Research*, **57**(2), Feb., pp. 143–154.
- [31] Hammerschlag, N., Gallagher, A. J., and Lazarre, D. M., 2011. "A review of shark satellite tagging studies". *Journal of Experimental Marine Biology and Ecology*, **398**(1), Feb., pp. 1–8.